On the dynamics and reversibility of the deactivation of a Rh/CeO_2-ZrO_2 catalyst in raw bio-oil steam reforming

Aingeru Remiro[a,*], Aitor Ochoa[a], Aitor Arandia[a,b], Pedro Castaño[a], Javier Bilbao[a] and Ana G. Gayubo[a]

[a]*Department of Chemical Engineering, University of the Basque Country (UPV/EHU), P.O. Box 644-48080, Bilbao, Spain.*

[b]*Department of Chemical and Metallurgical Engineering, School of Chemical Engineering, Aalto University, Espoo, 02150, Finland*

[*]*e-mail: aingeru.remiro@ehu.eus Phone: +34946015361. Fax:+34946013500*

Abstract

The deactivation mechanism of a commercial Rh/CeO_2-ZrO_2 catalyst in raw bio-oil steam reforming has been studied by relating the evolution with time on stream of the bio-oil conversion and products yields and the physicochemical properties of the deactivated catalyst studied by XRD, TPR, SEM, XPS, TPO and TEM. Moreover, the reversibility of the different deactivation causes has been assessed by comparing the behavior and properties of the catalyst fresh and regenerated (by coke combustion with air). The reactions were carried out in an experimental device with two units in series: a thermal treatment unit (at 500 ºC, for separation of pyrolytic lignin) and a fluidized bed reactor (at 700 ºC, for the reforming reaction). The results evidence that structural changes (support aging involving partial occlusion of Rh species) are irreversible and occur rapidly,-being responsible for a first deactivation period, whereas encapsulating coke deposition (with oxygenates as precursors) is reversible and evolves more slowly, thus being the main cause of the second deactivation period. The deactivation selectively affects the reforming of oxygenates, from least to greatest reactivity. Rh sintering is not a significant deactivation cause at the studied temperature.

Keywords: bio-oil, hydrogen, steam reforming, Rh catalyst, deactivation

1. Introduction

The development of thermochemical routes for sustainable H_2 production from biomass receives a great attention [1], in order to satisfy the increasing H_2 demand in ammonia production (fertilizers), in refinery (hydrotreatment and hydrocracking) and as a fuel [2]. Among these routes, the reforming of bio-oil (liquid product from fast pyrolysis of lignocellulosic biomass) is of great interest because the pyrolysis may be performed in delocalized units with different biomass types, with a simple design and environmentally friendly [3-4]. The stoichiometry of SR of bio-oil reaction is given by Eq. (1) (which involves the water gas shift (WGS) reaction):

$$C_nH_mO_k + (2n-k)\ H_2O \rightarrow\ n\ CO_2 + (2n+m/2-k)\ H_2 \quad (1)$$

Under suitable reaction conditions, it generates a product stream composed roughly of 70 % of H_2, 26 % of CO_2 and 4 % of CO [5]. The interpretation of the results in SR of real bio-oil turns out more complex than that of the individual model compounds [6-9], due to the different reactivity of the oxygenates, the synergy of their corresponding reforming reactions and, particularly, to the rapid deactivation of the catalyst [10-12]. The main deactivation causes of the catalyst are the blockage of metallic sites due to deposition of encapsulating coke and the sintering of metal crystallites [10-12]. Since the principal cause of coke deposition is the repolymerization of some oxygenates in bio-oil (mainly phenol compounds), the use of a thermal step prior to the catalytic reactor, for the controlled polymerization of the pyrolytic lignin, can partially solve this problem [13-16].

In previous works, the authors have used this operation strategy, with two-steps in line, in order to study the effect of the operating conditions in the product distribution and the pathway of the oxidative steam reforming (OSR) of bio-oil using a commercial Rh/CeO_2-ZrO_2 catalyst [17,18]. This catalyst has been proved to be more stable than those prepared with Ni as active phase, being noteworthy a significantly lower sintering under OSR conditions [19]. Although OSR turns out appropriate for attaining an autothermal regime in the reactor and decreasing coke deposition (by partial combustion of coke precursors), H_2 yield is noticeably affected by partial combustion of H_2 and bio-oil oxygenates. It was also determined that the relative relevance of the deactivation causes (coking, support degradation and

sintering) is dependent on reaction conditions, with great incidence of steam concentration, temperature and conversion, and also that the relevance of the different deactivation causes varies along TOS. Given the complexity of catalyst deactivation with several causes of different dynamics, the analysis of the evolution of catalyst properties along time on stream and its relationship with the evolution of catalysts behavior along the reaction will be of great help for deepening into the catalyst deactivation mechanism. Moreover, it is important to avoid the non-reversible deactivation causes, so that after a suitable regeneration treatment the catalyst recovers the activity of the fresh catalyst, allowing this way to extend the lifespan in successive reaction-regeneration cycles.

With this background, two main objectives have been pursued in this manuscript in order to study the deactivation of Rh/CeO_2-ZrO_2 catalyst in bio-oil SR. On the one hand, in order to gain more knowledge into the deactivation mechanism, the evolution with TOS of the kinetic behavior of the catalyst has been related with the deterioration of its properties. For this purpose, the catalysts deactivated for different values of TOS have been characterized in depth by combining several techniques for determining catalyst properties: the porous structure (N_2 adsorption-desorption), the coke features (Temperature Programmed Oxidation (TPO)), the metallic species (X-ray diffraction (XRD), Temperature Programmed Reduction (TPR), X-ray Photoelectron Spectroscopy (XPS)) and surface morphology (Scanning Electron Microscopy (SEM), Transmission Electron Microscopy (TEM)). These results have allowed relating the activity loss with the physical, chemical and morphologic changes in the catalyst throughout the reaction. On the other hand, the reversibility of the different deactivation causes has been studied. For that purpose, both the kinetic performance in the SR of bio-oil and the properties of the regenerated catalyst (by coke combustion with air at 600 ºC) has been compared to those of the fresh catalyst.

2. Materials and Methods

2.1. Catalyst and characterization techniques

The Rh/CeO_2-ZrO_2 catalyst (hereafter denoted Rh/ZDC), with 2 wt % Rh, was supplied by *Fuel Cell Materials*. The physicochemical properties of the fresh, reduced, deactivated and regenerated catalyst

samples have been characterized with several techniques, as follows. The specific surface area, average pore diameter and pore volume were determined by N_2 adsorption-desorption (*Autosorb iQ2* equipment from *Quantachrome)*. The TPR profiles were obtained in a *Micromeritics AutoChem 2920* with a 50 cm^3/min reducing stream of 10 vol % H_2/Ar mixture, and a heating ramp of 7 ºC/min from 30 to 900 ºC. The XRD spectra were obtained in a Philips X'PERT PRO diffractometer operating at 40 kV and 40 mA in theta-theta configuration with a secondary monochromator with CuKα1 radiation at a wavenumber of 1.5418 Å. An energy dispersive PIXcel detector was used with an active length of 2θ = 3.347 Å. The Rh particle size distribution (PSD) of the fresh and deactivated catalysts was estimated from TEM images, obtained in a *Philips SuperTwin CM200*, by counting more than 200 metal particles.

The XPS spectra were obtained using a SPECS (Berlin, Germany) system equipped with a Phoibos 150 1D-DLD analyzer, Al Kα monochromatic radiation (hν, 1486.6 eV), an X-ray exciting source, and a hemispherical electron analyzer. The binding energy of the C 1s carbon was set at 284.6 eV to correct the material charging, and the analysis was performed using an electron take off angle of 90°.

The coke on spent catalysts has been analyzed by Temperature Programmed Oxidation (TPO) in a *Thermo Scientific TGA Q5000TA* IR thermobalance. The procedure consisted on the stabilization of the sample temperature at 50 °C, followed by the feeding of 50 cm^3 min^{-1} of N_2 /O_2 (25 vol % of O_2) and the heating up to 800 °C with a ramp of 5 °C min^{-1}.

The morphology of the catalyst surface has been visualized by scanning electronic measure (SEM) in a JEOL JSM-7000F microscope with a tungsten filament (resolution 3.5 nm), operating at 20 kV, under vacuum at $9.65 \cdot 10^{-5}$ bar and intensity of $1.85 \cdot 10^{-10}$ A.

2.2. Bio-oil composition

The raw bio-oil was supplied by BTG Bioliquids BV (Hengelo, The Netherlands) and it was obtained by flash pyrolysis of pine sawdust in an plant with a capacity of 5 t h^{-1} and with a conical rotary reactor. The water content is 26 wt % (determined by Karl-Fischer), and its density is 1.105 g ml^{-1}. The composition, determined by GC/MS analysis (*Shimadzu QP2010S device,* with a *BPX-5* column of 50

m in length, 0.22 mm diameter and 0.25 μm thick), is reported in Table 1, being the main compounds: acids, ketones, phenols, levoglucosan, esters, aldehydes, alcohols, and ethers.

Table 1

2.3. Reaction equipment and operating conditions

The reactions were carried out with a continuous feed of raw bio-oil in an automated reaction equipment (*MicroActivity Reference* from *PID Eng&Tech*) with two units, which has been described in detail elsewhere [19]. In the first unit (thermal step, at 500 ºC) around 14.1 wt % of oxygenates in the raw bio-oil (water free basis) are deposited as pyrolytic lignin. Consequently, the composition of the bio-oil after the thermal treatment differs from that of the raw bio-oil, as shown in Table 1. The molecular formula of the treated bio-oil (that entering the reforming reactor) is $C_{4.12}H_{6.91}O_{2.73}$ (on a water-free basis) and that of the raw bio-oil is $C_{4.6}H_{6.2}O_{2.4}$. In the second unit in line (catalytic reforming reactor in fluidized bed regime), the catalyst is mixed with inert solid (SiC) (inert/catalyst mass ratio > 8/1) in order to ensure a correct fluidization regime. An injection pump *(Harvard Apparatus 22)* was used for feeding the bio-oil (0.08 ml/min), and the water was co-feed with a *307 Gilson pump*. The product stream composition was analyzed in-line with a *MicroGC 490* from *Agilent*, equipped with 4 analytic channels: molecular sieve MS5 (for H_2, N_2, O_2, CH_4 and CO); Plot Q (for CO_2, H_2O and C_2-C_4 hydrocarbons); CPSIL (for C_5-C_{11} hydrocarbons, which were not detected in this study), and; Stabilwax (for oxygenated compounds).

The catalyst is reduced in-situ (in a H_2-N_2 stream (10 vol % H_2) at 700 ºC for 2 h) before each reforming reaction. The following reforming conditions have been used: atmospheric pressure; 700 ºC; space time of 0.15 $g_{catalyst}h/g_{bio\text{-}oil}$; steam/carbon (S/C) molar ratio of 6. These values of temperature and S/C ratio are suitable for maximizing H_2 yield [17-19], whereas the low value of space time is suitable for obtaining a fast enough deactivation rate so that it facilitates the interpretation of results. At the end of each run a representative sample of the product stream at the reactor outlet has been condensed in a *Peltier* cell in order to analyze its composition in the CG/MS analyzer. Thus, the effect of deactivation on the composition of the stream of unreacted oxygenates was determined (selective deactivation).

Moreover, a reaction-regeneration cycle has been performed to test the recovery of activity and the properties of the catalyst. In this run, the reaction conditions have been those previously described (with 6 h TOS), and the regeneration has consisted in the coke combustion *in-situ* (in the reforming reactor) in air stream (50 ml/min) at 600 ºC for 4 h.

2.4. Quantification of catalyst behavior

The kinetic behavior of the catalyst has been quantified with the following terms:

Bio-oil conversion: $$X_{bio\text{-}oil} = \frac{F_{in} - F_{out}}{F_{in}} \quad (2)$$

H_2 yield: $$Y_{H_2} = \frac{F_{H_2}}{F^o_{H_2}} \quad (3)$$

Carbon-containing products yield: $$Y_i = \frac{F_i}{F_{in}} \quad (4)$$

where: F_{in} is the C molar flow-rate of oxygenates in the bio-oil at the reactor inlet, which has been calculated by subtracting the C in the pyrolytic lignin deposited in the thermal step to the C in the bio-oil fed to the system; F_{out} is the C molar flow-rate of bio-oil oxygenates at the outlet of the reactor, which has been calculated from the molar fraction of individual oxygenates (determined by microGC analysis) and the total mole number in the outlet stream (determined by C mass balance for the reforming reactor); F_{H2} is the H_2 molar flow rate in the product stream; F^0_{H2} is the stoichiometric molar flow rate, whose value is 2.18 F_{in} (calculated from Eq. (1) and considering the molecular formula of the bio-oil entering the reforming reactor); F_i is the C molar flow rate of each product containing carbon, which includes CO_2, CO, CH_4 and light hydrocarbons (HCs), the latter resulting from the cracking/decomposition reactions of bio-oil.

3. Results

3.1. Deactivation stages

Figure 1 shows the evolution with TOS of bio-oil conversion and product yields in SR of bio-oil, up to 360 min on stream. Taking into account the evolution of the results, five successive stages or catalyst deactivation states can be distinguished, with two sharp changes in the bio-oil conversion and products yields corresponding to different fast deactivation periods. The first period in Figure 1 (stage 1) corresponds to thermodynamic equilibrium conditions, with constant values of the bio-oil conversion and products yields (full bio-oil conversion and 0.95 of H_2 yield). Stage 2 corresponds to a short period of fast deactivation, which is followed by a new pseudostable state (stage 3), in which the catalyst still keeps high activity (0.95 of bio-oil conversion and around 0.7 of H_2 yield). Subsequently, a second fast catalyst deactivation period is observed (stage 4), with a rapid and more pronounced decrease in H_2 and CO_2 yields than that observed in the first deactivation period, and a parallel rapid increase in HCs yields. Once the catalyst has achieved a high deactivation level, the variation in the bio-oil conversion and products yields takes place slowly (stage 5) as they reach the values corresponding to thermal routes [17]. It is noteworthy that the catalyst keeps a residual activity for WGS reaction in stage 5, due to the ability of CeO_2-ZrO_2 support as a promoter of the Rh active sites [20,21].

Figure 1

The two different deactivation periods in Figure 1 give evidence of the existence of different deactivation causes, which have different dynamics. For a better identification of the deactivation causes and their dynamics, the catalyst deactivated for different values of TOS (selected because of their significance on the results shown in Figure 1) have been characterized in depth with the techniques described in Section 2.1. The selected TOS values are as follows: i) 50 min, prior to the first rapid deactivation period (state of incipient deactivation, with almost total conversion); ii) 100 min, at the end of the first rapid deactivation period. The comparison of the properties of this deactivated catalyst with those of fresh catalyst and that used for 50 min TOS will allow to ascertain the causes of the first deactivation period; iii) 240 min, just at the end of the intermediate pseudostable period (prior to the second deactivation period); iv) 360 min TOS, at the end of the reaction, corresponding to a highly deactivated catalyst. New runs of different duration (50, 100 and 240 min) have been performed in the conditions of Figure 1 in order to obtain the deactivated catalyst samples in these values of TOS. It is

noteworthy that the results of evolution with TOS of bio-oil conversion and products yields (Figure S1, Supplementary Information) confirm the reproducibility of the runs.

It is worth mentioning that, although the global conversion of the bio-oil oxygenates is considered in Figure 1, in fact, each oxygenated compound has a different reaction rate and is selectively affected by the deactivation. Table 1 shows the yield and mass composition of the liquid fraction (non-reacted oxygenates) in the product stream (dry basis) for different TOS values. These results allow determining the selective effect of deactivation in the reforming of the different families of bio-oil oxygenates. As observed, in conditions of incipient deactivation (50 min TOS, when the conversion is practically complete in Figure 1) the only oxygenates detected in the output stream are acetone and phenols, and just at the end of the first period of fast deactivation (100 min TOS), they are still the most abundant compounds, although the presence of other oxygenates begins to be remarkable, mainly acetic acid. The significant presence of phenols and acetone at a low TOS reveals the selective deactivation of the catalyst for the reforming of these compounds with respect to other oxygenates, due to their low reactivity. In addition, the high concentration of acetone at the beginning of the test could be a consequence of interconversion reactions of carboxylic acids, aldehydes and esters towards ketones, which seem to be highly favored at the beginning of the reaction, probably due to the activity of CeO_2-ZrO_2 support (especially of the latter) in the ketonization reactions [6,22,23]. The deactivation of the catalyst for the reforming of other oxygenates is already evident after 240 min TOS, when their presence in the liquid product is significant, with the concentration of acids and aldehydes (especially the former) being higher than those of esters and ethers. This way, as the catalyst gets more deactivated the composition of the liquid product resembles that of the thermally treated bio-oil, although some differences are expected because of some thermal interconversions of oxygenates occurs at 700 ºC in the fluidized bed reactor.

3.2. Coke deposition

The coke deposited on the deactivated samples has been studied by two techniques described in Section 2.1: i) TPO analysis, for determining the nature and location of the types of coke, based on their combustion temperature; ii) XPS analysis, for identifying and quantifying the functional groups of coke.

Figure 2 shows the TPO profiles of the catalyst samples spent at different values of TOS. A peak deconvolution of these profiles allows the identification of up to three coke types or fractions: coke Ia, with a peak maximum at ca. 275-310 ºC; coke Ib, 325-335 ºC; coke II, 360-410 ºC. According to the literature, the difference in the combustion temperature is mainly due to the differences in the chemical nature and coke location [17,24-31]. Thus, the peak at low combustion temperature (coke Ia) is amorphous and encapsulates the metallic sites, so that its combustion is catalyzed by these sites. The peak at intermediate combustion temperatures (coke Ib in Figure 2) is assigned to a coke fraction in the metal-support interface, that is, located further from metal sites and, thus, its combustion being partially catalyzed [18,32-36]. Finally, the peak at the highest combustion temperature (coke II) is ascribed to a coke fraction deposited on the catalyst support, which is further from metal sites and whose combustion is not catalytically activated. Moreover, this coke fraction usually possesses a significant amount of highly ordered polyaromatics, and is mainly formed from thermal decomposition mechanisms of oxygenates from bio-oil and reaction byproducts (mainly from light hydrocarbons) [27,29,30,37]. It should be noted that this allocation of the coke peaks, based on their relation with the metal sites, is based on the fact that the catalytic activation by the metal is the main cause of the different combustion temperature of the coke fractions. However, this interpretation may be partially masked by the different H/C ratio of the coke fractions, as the combustion is favored with an increase of H/C ratio [38].

Figure 2

In order to estimate the proportion of each coke type, the TPO profiles have been deconvoluted with Origin software and the results are summarized in Table 2, which include the following parameters: (i) the temperature of the each peak maximum (T_{max}); (ii) the percentage of each coke peak (wt% of the coke peak referred to the total coke mass); (iii) the content of each coke peak (wt% of the coke peak referred to the catalyst mass), (iv) and the total content of coke. The results show an increasing trend with TOS in the T_{max} values corresponding to the coke deposited on metal sites (coke Ia) and on the support (coke II), suggesting a carbonization process of these two coke fractions, which evolve with TOS by means of deoxygenation, dehydrogenation of aliphatics and aromatization [28,30,39]. The T_{max} corresponding to the coke deposited on the metal-support interface (coke Ib) remains almost constant

231 with TOS (at 330 ± 6 ºC), suggesting that its nature and location is not significantly altered during the
232 coking process.

233 The total coke content increases in an approximately linear trend, from 1.6 wt % at 50 min, up to 12.8
234 wt % at 360 min (Table 2). However, the percentage and content of each coke type evolve differently
235 with TOS. Thus, at lower values of TOS (up to 100 min), coke is preferentially deposited on the Rh sites
236 (coke Ia), involving a 90 wt % of the total coke (Table 2). Above 100 min, the deposition of coke on the
237 metal sites (coke Ia) continues, attaining a maximum content of 6.74 wt % at 240 min, but its percentage
238 within the total coke mass decreases (to 78 and 42 wt %, at 240 and 360 min, respectively), because
239 coke is more heterogeneously located and both the percentage and the content of the coke deposited on
240 the metal-support interface (coke Ib) and on the support (coke II) is increased. Thus, the percentage of
241 these latter coke fractions increases from 7 wt % (coke Ib) and 3 wt % (coke II) at 50 min, up to 37 wt
242 % (coke Ib) and 21 wt % (coke II) at 360 min. This increase in the heterogeneity of the coke is explained
243 because coke deposition takes place gradually further from the metal sites as they are being gradually
244 covered with coke. Moreover, the content of the coke deposited on the metallic sites (coke Ia) apparently
245 decreases above 240 min. This slight decrease could be the consequence not only of the location but
246 also of the composition (H/C ratio) of coke, and both have an influence on the position of combustion
247 peaks. Consequently, the slight decrease in coke Ia above 240 min could be also attributed to a partial
248 evolution towards more carbonized structures, which could contribute to the coke Ib combustion peak.
249 In any case, the difference of the results is small and can partially contribute to this difference the error
250 inherent to the identification of peaks by deconvolution.

251 **Table 2**

252 In order to examine the evolution of coke composition, the nature of the coke deposited on the catalysts
253 deactivated at different values of TOS was analyzed by XPS spectroscopy. Figure 3 shows the XPS
254 spectra in the C 1s region corresponding to the uppermost layers of surface coke. The corresponding
255 spectrum at 50 min is not shown, due to the low intensity (i.e. high noise-to-signal ratio) of the XPS
256 spectrum, because of the low coke content deposited at that time . The XPS profiles in Figure 3 have
257 been deconvoluted (with CasaXPS software) in five peaks, corresponding to different functional groups,

as indicated in Table 3 [27,40-42]. This table includes; i) the contributions (relative intensities) of these five bands (named *1* to *5*) with respect to the whole XPS spectrum; ii) the total concentration of the C 1s region with respect to the global spectrum, denoted as 'C 1s', which provides a rough comparison of the coke content in the uppermost layers of the deactivated catalyst; iii) the atomic contribution (%) of the bands 1 and 2 (assigned to a carbon atom not bonded to an oxygen atom) referred to the C 1s concentration (denoted as '(*1* + *2*)/C 1s'); iv) the atomic contribution (%) of the bands 3 and 4 (assigned to a carbon atom bonded to an oxygen atom) referred to the C 1s concentration (denoted as '(*3* + *4*)/C 1s'). The last two values allow to analyze the concentration of non-oxygenated and oxygenated coke, respectively.

Figure 3

Table 3

The results in Table 3 show that as TOS is increased, there is a higher surface carbon content, in line with the total content of coke deposited (Table 2), and the content of oxygenated bonds within coke (contribution of bands 3 and 4) is decreased. It is noteworthy that the percentage of coke type I (a and b) (97, 84 and 79 wt % at 100, 240 and 360 min, respectively (Table 2)), shows a similar trend with TOS to the oxygenated fraction of coke (values of 18.7, 14.2 and 13.8 % for '(*3* + *4*)/C 1s' in Table 3), suggesting that coke I is the main responsible for the oxygenated nature of the coke deposited. Thus, this result is coherent with the aforementioned statement that bio-oil oxygenates are the precursors of encapsulating coke (coke Ia), thus leading to a relatively highly hydrogenated and/or oxygenated nature (higher H/C and/or O/C ratio). The coke deposited on the metal-support interface (coke Ib) is also thought to contribute to the oxygenated nature of coke deposited, although to a lesser extent than coke Ia. Moreover, the lower combustion temperature of coke I (a and b) in the TPO profiles (Figure 2) is coherent with their oxygenated nature, as the combustion of carbonaceous materials is favored by the presence of oxygenated compounds, according to the literature [43,44].

3.3. Support deterioration (aging)

283 The surface properties (BET surface area, pore volume and mean pore diameter) for the Rh/ZDC catalyst
284 fresh, fresh-reduced and used for different TOS values are gathered in Table 4. The results show that
285 the BET surface area and pore volume undergo a noticeable deterioration during the reduction (before
286 the reaction) and this deterioration is even more noticeable during the reaction, especially in the first 50
287 min TOS. For these three samples, the mean pore diameter has an opposite trend, so that it increases
288 (more noticeably from the fresh to the fresh-reduced sample). The three surface properties decrease as
289 TOS increases from 50 to 360 min, the decrease in BET surface area and pore volume being more
290 noticeable between 100 min and 240 min TOS, whereas pore diameter decreases more noticeably
291 between 240 and 360 min TOS.

292 **Table 4**

293 The possible causes for this deterioration of the porous structure can be the aging of the support and the
294 deposition of coke. The comparison of the values for the fresh and the fresh-reduced sample evidences
295 the aging of the support due to the high temperature used for reducing the catalyst (700 ºC, for 2 h).
296 Moreover, taking into account the insignificant coke deposition at 50 min TOS (Table 2), the
297 deterioration of the physical properties at the beginning of the reaction should be attributed to a further
298 aging of the support under SR conditions (with a significant concentration of steam in the reaction
299 medium). It is noteworthy that the aging of the support involves an increase in pore diameter, which
300 gives evidence that it involves a collapse of the narrower pores. This significant aging of the support at
301 high temperature is coherent with previous results in literature for catalysts based on CeO_2 and CeO_2-
302 ZrO_2 [45,46]. In a previous work concerning OSR of bio-oil [18] it was proven that this deterioration
303 depends on the reaction conditions, being more noticeable as temperature is increased.

304 The similar values of the physical properties of the catalyst used for 50 and 100 min TOS evidences that
305 there is not a further aging of the support with TOS. Nevertheless, BET surface area, pore volume and
306 pore diameter decrease noticeably between 100 and 240 min, with this decrease being parallel to the
307 noticeable increase in coke deposition (both encapsulating and structured coke) observed in Figure 2.

Consequently, it can be concluded that coke deposition also contributes to the deterioration of the physical properties of the catalyst, although to a much lower extent than the aging of the support.

The SEM images shown in Figure S2 of Supplementary Information for the catalyst fresh and used for different TOS values (50, 100 and 360 min) corroborates the results obtained by N_2 adsorption-desorption. Thus, although this technique does not allow observing notable differences between the catalyst samples, in the fresh catalyst (Figure S2a) it is observed a granular surface, whereas the catalyst at 50 min TOS (Figure S2b) possesses flatter surface regions with a lower porosity, which evidences the support aging for this TOS value. The SEM images of deactivated catalyst for high TOS (Figures S2c-d) are similar to those of 50 min, which corroborates that support aging takes place at the beginning of the reaction.

Figure 4 shows the XRD spectra of the fresh catalyst and deactivated at different TOS. The results confirm the presence of mixed oxide $Ce_xZr_{1-x}O_2$, but no diffraction peaks corresponding to oxidized or reduced Rh species are observed, because of the low content and high dispersion of Rh on the support [19]. The mixed oxide of the support does not show any significant variation with TOS, as the crystallite size remains constant between 9.8 and 10.8 nm (plane 1 1 1, θ = 29.2 º), calculated by the Scherrer equation. Therefore, sintering of the support is not significant and hence, it is not responsible of catalyst deactivation at studied conditions.

Figure 4

3.4. Changes in the Rh species

The evolution with TOS of the oxidation state of Rh species has been explored by XPS analysis of the fresh-reduced and the deactivated catalysts. In order to avoid the oxidation of the samples prior to XPS analysis, they were passivated in isooctane after being removed from the reactor. Figure 5 shows the XPS spectra in the Rh 3d region, deconvoluted in four bands [47-49]: (1) Rh $3d_{5/2}$ spin-orbit doublet for Rh^0, 307.4 eV; (2) that for Rh^{3+}, 309.2 eV; (3) Rh $3d_{3/2}$ spin-orbit doublet for Rh^0, 312.2 eV; (4) that for Rh^{3+}, 313.8 eV. Table 5 gathers the relative intensities of the four mentioned bands with respect to the whole XPS spectrum, as well as the evolution with TOS of the oxidation level of Rh, named 'Rh^{3+}/Rh^0',

334 which has been calculated from the ratio between the sum of deconvoluted areas below Rh^{3+} and Rh^0
335 phases. The results for 360 min TOS are not displayed in Figure 5 and Table 5, as no Rh phases were
336 observed in the surface due to the high coke content deposited on the surface at that TOS and the limited
337 detection depth (< 10 nm) of XPS technique [49].

338 **Figure 5**

339 **Table 5**

340 The reduced fresh catalyst (TOS = 0) only shows the Rh^0 phase ($Rh^{3+}/Rh^0 = 0$), whereas the oxidized
341 proportion of Rh during the reaction increases with TOS, from a Rh^{3+}/Rh^0 ratio of 0.13 at 50 min, up to
342 1.18 at 240 min, with the maximum oxidation rate in the region between 50 min and 100 min. This
343 progressive oxidation of Rh with TOS is due to the reaction medium with a high content of water, 80
344 wt %. Comparing this result with the evolution of bio-oil conversion and products yields with TOS
345 (Figure 1), it is observed that this oxidation of Rh occurs mainly in parallel to the first rapid decrease in
346 the catalyst activity (stage 2 in Figure 1), so that it could contribute to some extent to the deactivation
347 observed in this period (which is mainly due to the aging of the support and the corresponding partial
348 occlusion of Rh species, phenomena studied in Section 3.3).
349 The growth of the Rh particle size along TOS has been studied by TEM analysis, in order to determine
350 Rh sintering dynamics, and its possible contribution to catalyst deactivation. Figure 6 shows the TEM
351 images of samples deactivated at different TOS values, whereas Figure 7 depicts the evolution with TOS
352 of the particle size distribution (PSD) of the deactivated catalyst samples and the average size for each
353 sample, calculated as the arithmetic mean of more than 200 particles. The average size is 1.4 nm for the
354 fresh catalyst, it grows slightly and almost linearly up to 1.8 nm in 100 min, and subsequently the growth
355 is attenuated, up to 2.1 nm at 360 min, and up to 2.2 nm in 24 h [18]. Moreover, the width of the PSD
356 does not change significantly with TOS. This level of Rh sintering at 700 ºC (particle size of fresh-
357 reduced catalyst grows 55 % in 360 min), agrees with previous results in literature for Rh particles
358 supported on CeO_2 [50,51]. The trend of Rh particle size growth with TOS does not show a direct
359 relationship with none of the deactivation periods observed in Figure 1 (stages 2 and 4), which proves

360 that it does not significantly contribute to Rh/ZDC catalyst deactivation in the studied conditions (at 700
361 ºC).

362 **Figure 6**

363 **Figure 7**

364 *3.5. Performance and properties of the regenerated catalyst*

365 In order to analyze the reversibility and relative importance of the different deactivation causes, the
366 catalyst deactivated along 360 min TOS has been regenerated *in situ* (in the fluidized bed reactor) by
367 coke combustion with air at 600 ºC for 4 h (in order to assure the complete coke removal), and a run
368 with the regenerated catalyst has been carried out under the same operating conditions as with the fresh
369 catalyst. Figure 8 shows the evolution with TOS of bio-oil conversion and products yields with the
370 regenerated catalyst. At zero TOS, conversion is 93 % and H_2 yield 71 %, lower values than those
371 obtained with the fresh catalyst at zero TOS (100 % and 95 %, respectively, Figure 1), and they are
372 similar to those obtained with the fresh catalyst at 100 min, at the beginning of the pseudostable period
373 (stage 3 in Figure 1). Likewise, the yields of CH_4 and HCs (Figure 8) at zero TOS for the regenerated
374 catalyst are also similar to those obtained with the fresh catalyst at 100 min. Moreover, the regenerated
375 catalyst only shows one deactivation period, whose magnitude is similar to that of the second
376 deactivation period observed for the fresh catalyst. Consequently, CH_4 yield remains constant at approx.
377 6 % throughout the reaction with the regenerated catalyst, whereas H_2 and CO_2 yields decrease sharply
378 after a pseudostable period, and that of HCs increases. CO yield goes through a maximum with TOS for
379 both the fresh and the regenerated catalysts, even though the maximum is achieved at different TOS for
380 each catalyst. This evolution of CO yield is consequence of the opposed effects of the deactivation of
381 WGS reaction (leading to CO increase) and the deactivation of the reforming of HCs and oxygenates
382 (CO decrease), as well as the selective deactivation of WGS reaction over HCs and oxygenates
383 reforming reactions.

384 **Figure 8**

These results reveal a partial regeneration of the Rh/ZDC catalyst subsequent to the complete removal of the coke deposited on its surface. Specifically, the loss of activity in the first deactivation stage, assigned to aging of the support, is not recovered, which evidences that it is an irreversible deactivation. On the contrary, the deactivation stage ascribed to the deposition of encapsulating coke is reversible, since the activity loss in the second deactivation period is completely recovered subsequent to coke combustion.

With the aim of corroborating the irreversible nature of the structural changes in the catalyst, the regenerated catalyst has been characterized by several techniques (TPR, XPS and adsorption-desorption of N_2). Figure 9 shows the TPR profiles of the fresh and regenerated catalysts, and the results evidence a change in the Rh structure. On the one hand, the reduction peak at 200 ºC in the fresh catalyst (ascribed by some authors to a bulk-like crystalline Rh_2O_3 on the surface (large particles) [18]) is absent in the regenerated catalyst. This disappearance of Rh reducible species may be explained by their partial occlusion due to the aging of the support. On the other hand, the position of the peak ascribed to the reduction of well-dispersed and uniformly distributed rhodium oxides shifts toward higher temperature (from 65 to 98 ºC), which may be due to the mild increase in the metallic particle size [49,52].

Figure 9

Furthermore, the regenerated catalyst shows a BET specific area of 40.5 $m^2\ g^{-1}$ and a pore volume and average pore diameter of 0.212 $cm^3\ g^{-1}$ and 20.9 nm, respectively, which are significantly lower than those corresponding to the fresh catalyst (Table 4), and similar to those of the catalyst deactivated for 50-100 TOS values. These results evidence that aging of the support at the beginning of the reaction (in the first 50 min) is irreversible. Nevertheless, the BET surface area and pore volume of the regenerated catalyst are significantly higher than those of the catalyst used for 360 min TOS, which evidences that the slight deterioration of the support taking place between 100-360 min TOS, assigned to coke deposition, is reversible. Moreover, taking into account the irreversibility of Rh sintering, the complete recovery of the activity lost during the second deactivation period for the regenerated catalyst reinforces the conclusion that Rh sintering is not responsible for the activity loss in this period (which is completely reversible).

412 The XPS spectra in the Rh 3d region for the regenerated-reduced catalyst shows only two peaks at 307.4
413 and 312.2 eV (Table 5), corresponding to Rh^0-$3d_{5/2}$ and Rh^0-$3d_{5/2}$, respectively, which evidences that the
414 oxidized Rh species in the regenerated catalyst can be completely reduced. From these results, it can be
415 concluded that Rh oxidation is not responsible of the irreversible activity loss occurring in the first
416 deactivation period and, overall, it has low impact on catalyst deactivation.

417 It is worth noting that the irreversible deactivation phenomena only affects the fresh catalyst, as in
418 successive reaction-regeneration cycles the evolution with TOS of bio-oil conversion and products
419 yields are reproduced, (results not shown). Consequently, when operating in reaction-regeneration
420 cycles with this catalyst at a larger scale, the most interesting deactivation results will be those
421 corresponding to coke deposition. The problem of the first irreversible deactivation period in the SR of
422 raw bio-oil with Rh/ZDC catalyst could be avoided by subjecting the catalyst to a prior hydrothermal
423 treatment, at high temperature and with high steam concentration, which causes the irreversible
424 structural changes observed for low values of TOS, thus assuring a reproducible performance in
425 successive reaction–regeneration cycles.

426 **5. Conclusions**

427 The results of the characterization of the Rh/ZDC catalyst deactivated in the SR of bio-oil for different
428 TOS values show changes in the physicochemical and morphological properties of the catalyst along
429 the reaction, which are due to three deactivation causes: structural changes, coke deposition and Rh
430 sintering. Each deactivation cause evolves with different dynamics and has a different impact on catalyst
431 deactivation and, as a result, two different deactivation periods are observed. The first deactivation
432 selectively affects the reforming of CH_4 and some oxygenates (mainly phenols), whereas the reforming
433 of HCs and other oxygenates are less affected. It is a consequence of a structural change of the catalyst,
434 which is complex (involving changes in Rh species as a consequence of the aging of the support) and
435 occurs rapidly at the beginning of reaction, when catalyst is subjected at severe reaction conditions (high
436 temperature and high steam concentration). This structural change is irreversible, so that the activity
437 loss in this first deactivation period cannot be recovered subsequent to the regeneration of the catalyst
438 by coke combustion. Moreover, at the beginning of the reaction a partial oxidation from Rh^0 to Rh^{3+}also

takes place, which is completely reversible and has low impact on catalyst deactivation. It should be noted that this deactivation phenomenon is selective. The rapid appearance of phenols in product stream, and subsequent other oxygenates, reveals that deactivation affects the reforming of oxygenates from least to greatest reactivity.

The second deactivation period is mainly due to the deposition of encapsulating coke (located on the metal sites, with non-converted oxygenates, mainly phenolic compounds, as precursors), which is a reversible deactivation cause, as it can be completely removed by coke combustion at 600 ºC. The coke deposited on metal-support interface and on the support has low effect on deactivation. Similarly, Rh sintering does not contribute significantly to catalyst deactivation, as it is an emerging deactivation cause at the studied temperature (700 ºC).

Acknowledgements

This work was carried out with the financial support of the Department of Education Universities and Investigation of the Basque Government (IT748-13), the Ministry of Economy and Competitiveness of the Spanish Government jointly with the European Regional Development Funds (AEI/FEDER, UE) (Proyects CTQ2015-68883-R and CTQ2016-79646-P and Ph.D. grant BES-2013-063639 for A. Arandia and Ph.D. grant PRE_2016_2_0129 for A. Ochoa).

References

[1] A. Arregi, M. Amutio, G. Lopez, J. Bilbao, M. Olazar, Evaluation of thermochemical routes for hydrogen production from biomass: A review, Energy Convers. Manage. 165 (2018) 696–719. https://doi.org/10.1016/j.enconman.2018.03.089

[2] A.M. Abdalla, S. Hossain, O.B. Nisfindy, A.T. Azad, M. Dawood, A.K. Azad, Hydrogen production, storage, transportation and key challenges with applications: A review, Energy Convers. Manage. 165 (2018) 602–627. https://doi.org/10.1016/j.enconman.2018.03.088

[3] G. Perkins, T. Bhaskar, M. Konarova, Process development status of fast pyrolysis technologies for the manufacture of renewable transport fuels from biomass, Renew. Sust. Energ. Rev. 90 (2018) 292–315. https://doi.org/10.1016/j.rser.2018.03.048

[4] A.V. Bridgwater, Review of fast pyrolysis of biomass and product upgrading, Biomass Bioenergy 38 (2012) 68–94. https://doi.org/10.1016/j.biombioe.2011.01.048

[5] S. Czernik, R. Evans, R. French, Hydrogen from biomass-production by steam reforming of biomass pyrolysis oil, Catal. Today 129 (2007) 265–268. https://doi.org/10.1016/j.cattod.2006.08.071

[6] A.A. Lemonidou, E.C. Vagia, J.A. Lercher, Acetic acid reforming over Rh supported on $La_2O_3/CeO_2–ZrO_2$: catalytic performance and reaction pathway analysis, ACS Catal. 3 (2013) 1919–1928. https://doi.org/10.1021/cs4003063

[7] D. Li, X. Li, J. Gong, Catalytic reforming of oxygenates: State of the art and future prospects, Chem. Rev. 116 (2016) 11529–11653. https://doi.org/10.1021/acs.chemrev.6b00099

[8] G. Chen, J. Tao, C. Liu, B. Yan, W. Li, X. Li, Hydrogen production via acetic acid steam reforming: A critical review on catalysts, Renew. Sust. Energ. Rev. 79 (2017) 1091–1098. https://doi.org/10.1016/j.rser.2017.05.107

[9] W. Nabgan, T.A.T. Abdullah, R. Mat, B. Nabgan, A.A. Jalil, L. Firmansyah, S. Triwahyono, Production of hydrogen via steam reforming of acetic acid over Ni and Co supported on La_2O_3 catalyst, Int. J. Hydrogen Energy 42 (2017) 8975–8985. https://doi.org/10.1016/j.ijhydene.2016.04.176

[10] R. Trane, S. Dahl, M.S. Skjoth-Rasmussen, A.D. Jensen, Catalytic steam reforming of bio-oil, Int. J. Hydrogen Energy 37 (2012) 6447–6472. https://doi.org/10.1016/j.ijhydene.2012.01.023

[11] T. Kan, J. Xiong, X. Li, T. Ye, L. Yuan, Y. Torimoto, M. Yamamoto, Q. Li, High efficient production of hydrogen from crude bio-oil via an integrative process between gasification and current-enhanced catalytic steam reforming, Int. J. Hydrogen Energy 35 (2010) 518–532. https://doi.org/10.1016/j.ijhydene.2009.11.010

[12] F. Seyedeyn-Azad, E. Salehi, J. Abedi, T. Harding, Biomass to hydrogen via catalytic steam reforming of bio-oil over Ni-supported alumina catalysts, Fuel Process. Technol. 92 (2011) 563–569. https://doi.org/10.1016/j.fuproc.2010.11.012

[13] A.G. Gayubo, B. Valle, A.T. Aguayo, M. Olazar, J. Bilbao, Pyrolytic lignin removal for the valorization of biomass pyrolysis crude bio-oil by catalytic transformation, J. Chem. Technol. Biotechnol. 85 (2010) 132–144. https://doi.org/10.1002/jctb.2289

[14] A. Remiro, B. Valle, A.T. Aguayo, J. Bilbao, A.G. Gayubo, Steam reforming of raw bio-oil in a fluidized bed reactor with prior separation of pyrolytic lignin, Energy Fuels 27 (2013) 7549–7559. https://doi.org/10.1021/ef401835s

[15] B. Valle, A. Remiro, B. Aramburu, J. Bilbao, A.G. Gayubo, Strategies for maximizing the bio-oil valorization by catalytic transformation, J. Clean. Prod. 88 (2015) 345–348. https://doi.org/10.1016/j.jclepro.2014.06.017

[16] B. Valle, B. Aramburu, A. Arandia, A. Remiro, J. Bilbao, A.G. Gayubo, Optimal conditions of thermal treatment unit for the steam reforming of raw bio-oil in a continuous two-step reaction system, Chem. Eng. Trans. 57 (2017) 205–2010. https://doi.org/10.3303/CET1757035

[17] A. Arandia, A. Remiro, L. Oar-Arteta, J. Bilbao, A.G. Gayubo, Reaction conditions effect and pathways in the oxidative steam reforming of raw bio-oil on a Rh/CeO_2-ZrO_2 catalyst in a fluidized bed reactor, Int. J. Hydrogen Energy 42 (2017) 29175–29185. https://doi.org/10.1016/j.ijhydene.2017.10.095

[18] A. Remiro, A. Arandia, L. Oar-Arteta, J. Bilbao, A.G. Gayubo, Stability of a Rh/CeO_2-ZrO_2 catalyst in the oxidative steam reforming of raw bio-oil, Energy Fuels 32 (2018) 3588–3598. https://doi.org/10.1021/acs.energyfuels.7b04141

[19] A. Remiro, A. Arandia, J. Bilbao, A.G. Gayubo, Comparison of Ni Based and Rh Based Catalyst Performance in the Oxidative Steam Reforming of Raw Bio-Oil, Energy Fuels 31 (2017) 7147–7156. https://doi.org/10.1021/acs.energyfuels.7b00735

[20] H-S. Roh, H.S. Potdar, D-W. Jeong, K-S. Kim, J-O. Shim, W-J. Jang, K.Y. Koom, W.L. Yoon, Synthesis of highly active nano-sized (1 wt.% Pt/CeO_2) catalyst for water gas shift reaction in medium temperature application, Catal. Today 185 (2012) 113–118. https://doi.org/10.1016/j.cattod.2011.10.016

[21] S. Aranifard, S.C. Ammal, A. Heyden, On the importance of metal–oxide interface sites for the water–gas shift reaction over Pt/CeO_2 catalysts, J. Catal. 309 (2014) 3–324. https://doi.org/10.1016/j.jcat.2013.10.012

[22] C.A. Gaertner, J.C. Serrano-Ruiz, D.J. Braden, J.A. Dumesic, Ketonization reactions of carboxylic acids and esters over ceria−zirconia as biomass-upgrading processes, Ind. Eng. Chem. Res. 49 (2010) 6027–6033. https://doi.org/10.1021/ie1004338

[23] Y. Yamada, M. Segawa, F. Sato, T. Kojima, S. Sato, Catalytic performance of rare earth oxides in ketonization of acetic acid, J. Mol. Catal. A 346 (2011) 79–86. https://doi.org/10.1016/j.molcata.2011.06.011

[24] B. Valle, B. Aramburu, M. Olazar, J. Bilbao, A.G. Gayubo, Steam reforming of raw bio-oil over Ni/La_2O_3-αAl_2O_3: Influence of temperature on product yields and catalyst deactivation, Fuel 216 (2018) 463–474. https://doi.org/10.1016/j.fuel.2017.11.149

[25] B. Valle, B. Aramburu, P.L. Benito, J. Bilbao, A.G. Gayubo, Biomass to hydrogen-rich gas via steam reforming of raw bio-oil over Ni/La_2O_3-αAl_2O_3 catalyst: Effect of space-time and steam-to-carbon ratio, Fuel 216 (2018) 445–455. https://doi.org/10.1016/j.fuel.2017.11.151

[26] N. Martin, M. Viniegra, E. Lima, G. Espinosa, Coke Characterization on Pt/Al_2O_3−β-Zeolite Reforming Catalysts, Ind. Eng. Chem. Res. 43 (2004) 1206–1210. https://doi.org/10.1021/ie034007b

[27] A. Ochoa, B. Aramburu, B. Valle, D.E. Resasco, J. Bilbao, A.G. Gayubo, P. Castaño, Role of oxygenates and effect of operating conditions in the deactivation of a Ni supported catalyst during the steam reforming of bio-oil, Green Chem. 19 (2017) 4315–4333. https://doi.org/10.1039/C7GC01432E

[28] A. Ochoa, I. Barbarias, M. Artetxe, A.G. Gayubo, M. Olazar, J. Bilbao, P. Castaño, Deactivation dynamics of a Ni supported catalyst during the steam reforming of volatiles from waste polyethylene pyrolysis, Appl. Catal. B 209 (2017) 554–565. https://doi.org/10.1016/j.apcatb.2017.02.015

[29] A. Ochoa, B. Aramburu, B. Valle, D.E. Resasco, J. Bilbao, A.G. Gayubo, P. Castaño, TPO coupled with in-situ techniques reveal nature and location of coke deposited on a Ni/La_2O_3-αAl_2O_3 catalyst in the steam reforming of bio-oil, ChemCatChem 10 (2018) 1–12. https://doi.org/10.1002/cctc.201701942.

[30] A. Ochoa, A. Arregi, M. Amutio, A.G. Gayubo, M. Olazar, J. Bilbao, P. Castaño, Coking and sintering progress of a Ni supported catalyst in the steam reforming of biomass pyrolysis volatiles, Appl. Catal. B 233 (2018) 289-300. https://doi.org/10.1016/j.apcatb.2018.04.002

[31] C. Montero, A. Ochoa, P. Castaño, J. Bilbao, A.G. Gayubo, Monitoring Ni^0 and coke evolution during the deactivation of a Ni/La_2O_3–αAl_2O_3 catalyst in ethanol steam reforming in a fluidized bed, J. Catal. 331 (2015) 181–192. https://doi.org/10.1016/j.jcat.2015.08.005

[32] B. Valle, A. Remiro, A.T. Aguayo, J. Bilbao, A.G. Gayubo, Catalysts of Ni/αAl_2O_3 and Ni/La_2O_3-αAl_2O_3 for hydrogen production by steam reforming of bio-oil aqueous fraction with pyrolytic lignin retention, Int. J. Hydrogen Energy 38 (3) (2013) 1307–1318. https://doi.org/10.1016/j.ijhydene.2012.11.014

[33] A. Remiro, B. Valle, B. Aramburu, A.T. Aguayo, J. Bilbao, A.G. Gayubo, Steam reforming of the bio-oil aqueous fraction in a fluidized bed reactor with in situ CO_2 capture, Ind. Eng. Chem. Res. 52 (48) (2013) 17087–17098. https://doi.org/10.1021/ie4021705

[34] A. Remiro, B. Valle, A.T. Aguayo, J. Bilbao, A.G. Gayubo, Operating conditions for attenuating Ni/La_2O_3-αAl_2O_3 catalyst deactivation in the steam reforming of bio-oil aqueous fraction, Fuel Process. Technol. 115 (2013) 222–232. https://doi.org/10.1016/j.fuproc.2013.06.003

[35] J. Ereña, I. Sierra, M. Olazar, A.G. Gayubo, A.T. Aguayo, Deactivation of a CuO-ZnO-Al_2O_3/γ-Al_2O_3 catalyst in the synthesis of dimethyl ether. Ind. Eng. Chem. Res. 47 (2008) 2238−2247. https://doi.org/10.1021/ie071478f

[36] A.G. Gayubo, J. Vicente, J. Ereña, L. Oar-Arteta, M.J. Azkoiti, M. Olazar, J. Bilbao, Causes of deactivation of bifunctional catalysts made up of CuO-ZnO-Al_2O_3 and desilicated HZSM-5 zeolite in DME steam reforming, Appl. Catal. A 483 (2014) 76–84. https://doi.org/10.1016/j.apcata.2014.06.031

[37] J. Vicente, J. Ereña, C. Montero, M.J. Azkoiti, J. Bilbao, A.G. Gayubo, Reaction pathway for ethanol steam reforming on a Ni/SiO_2 catalyst including coke formation, Int. J. Hydrogen Energy, 39 (2014) 18820–18834. https://doi.org/10.1016/j.ijhydene.2014.09.073

[38] J.M. Ortega, A.G. Gayubo, A.T. Aguayo, P.L. Benito, J. Bilbao. Role of coke characteristics in the regeneration of a catalyst for the MTG process. Ind. Eng. Chem. Res. 36 (1997) 60–66. https://doi.org/10.1021/ie9507336

[39] J. Vicente, C. Montero, J. Ereña, M.J. Azkoiti, J. Bilbao, A.G. Gayubo, Coke deactivation of Ni and Co catalysts in ethanol steam reforming at mild temperatures in a fluidized bed reactor, Int. J. Hydrogen Energy 39 (2014) 12586–12596. https://doi.org/10.1016/j.ijhydene.2014.06.093

[40] J.F. Watts, J. Wolstenholme, An introduction to surface analysis by XPS and AES, John Wiley & Sons, West Sussex, England, UK, 2003.

[41] H. Estrade-Szwarckopf, XPS photoemission in carbonaceous materials: A “defect” peak beside the graphitic asymmetric peak, Carbon 42 (2004) 1713–1721. https://doi.org/10.1016/j.carbon.2004.03.005

[42] A. Ochoa, B. Aramburu, M. Ibáñez, B. Valle, J. Bilbao, A.G. Gayubo, P. Castaño, Compositional insights and valorization pathways for carbonaceous material deposited during bio-oil thermal treatment, ChemSusChem 7 (2014) 2597–2608. https://doi.org/10.1002/cssc.201402276

[43] X. Liu, M. Chen, D. Yu, Oxygen enriched co-combustion characteristics of herbaceous biomass and bituminous coal, Thermochim. Acta 569 (2013) 17–24. https://doi.org/10.1016/j.tca.2013.06.037

[44] J. Abboud, J. Schobing, G. Legros, J. Bonnety, V. Tschamber, A. Brillard, G. Leyssens, V. Lauga, E.E. Iojoiu, P. Da Costa, Impacts of oxygenated compounds concentration on sooting propensities

and soot oxidative reactivity: Application to diesel and biodiesel surrogates, Fuel 193 (2017) 241–253. https://doi.org/10.1016/j.fuel.2016.12.034

[45] P. Pantu, G.R. Gavalas, Methane partial oxidation on Pt/CeO_2 and Pt/Al_2O_3 catalysts, Appl. Catal. A 223 (2002) 253–260. https://doi.org/10.1016/S0926-860X(01)00761-X

[46] V.B. Mortola, J.A.C. Ruiz, L.V. Mattos, F.B. Noronha, C.E. Hori, Partial oxidation of methane using $Pt/CeZrO_2/Al_2O_3$ catalyst—Effect of the thermal treatment of the support, Catal. Today 133–135 (2008) 906–912. https://doi.org/10.1016/j.cattod.2007.12.067

[47] J. Kugai, V. Subramani, C. Song, M.H. Engelhard, Y. Chin, Effect of nanocrystalline CeO_2 supports on the properties and performance of Ni-Rh bimetallic catalyst for oxidative steam reforming of ethanol, J. Catal. 238 (2006) 430–440. https://doi.org/10.1016/j.jcat.2006.01.001

[48] X. Han, Y. Yu, H. He, W. Shan, Hydrogen production from oxidative steam reforming of ethanol over rhodium catalysts supported on Ce-La solid solution, Int. J. Hydrogen Energy, 38 (2013) 10293–10304. https://doi.org/10.1016/j.ijhydene.2013.05.137

[49] Y. Cao, R. Ran, X. Wu, X. Wu, J. Wan, D. Weng, Ageing resistance of rhodium supported on CeO_2-ZrO_2 and ZrO_2: Rhodium nanoparticle structure and Rh-support interaction under diverse ageing atmosphere, Catal. Today 281 (2017) 490–499. https://doi.org/10.1016/j.cattod.2016.07.001

[50] P. Osorio-Vargas, C.H. Campos, R.M. Navarro, J.L.G. Fierro, P. Reyes, Improved ethanol steam reforming on Rh/Al_2O_3 catalysts doped with CeO_2 or/and La_2O_3: Influence in reaction pathways including coke formation, Appl. Catal. A 505 (2015) 159–172. https://doi.org/10.1016/j.apcata.2015.07.037

[51] T. Hou, B. Yu, S. Zhang, T. Xu, D. Wang, W. Cai, Hydrogen production from ethanol steam reforming over Rh/CeO_2 catalyst, Catal. Commun. 58 (2015) 137–140. https://doi.org/10.1016/j.catcom.2014.09.020

[52] C. Diagne, H. Idriss, A. Kiennemann, Hydrogen production by ethanol reforming over Rh/CeO_2-ZrO_2 catalysts, Catal. Commun. 3 (2002) 565–571. https://doi.org/10.1016/S1566-7367(02)00226-1

621 **Figure Captions**

622 **Figure 1.** Evolution with TOS of bio-oil oxygenates conversion and yields of products and
623 deactivation stages in the SR of bio-oil with Rh/CeO_2-ZrO_2 catalyst. Reaction conditions:
624 700 ºC; S/C, 6; space time, 0.15 $g_{catalyst}/g_{bio\text{-}oil}$ h.

625 **Figure 2.** Deconvolution of TPO profiles corresponding to coke deposited on the catalyst at different
626 values of TOS.

627 **Figure 3.** C 1s region in the XPS spectra of the deactivated catalyst at different values of TOS.

628 **Figure 4.** XRD diffractograms of the deactivated catalysts at different TOS.

629 **Figure 5.** Rh 3d region in the XPS spectra of the reduced fresh and deactivated catalysts at different
630 TOS.

631 **Figure 6.** TEM images of fresh catalyst (a,b) and of deactivated catalysts at different TOS: 50 min (c),
632 100 min (d), 240 min (e) and 360 min (f).

633 **Figure 7.** Particle size distribution (PSD) of fresh catalyst and of deactivated catalysts at different TOS.

634 **Figure 8.** Evolution with TOS of conversion and yield of products in the SR of raw bio-oil over the
635 regenerated catalyst. Reaction conditions: the same as in Figure 1. Regeneration conditions:
636 coke combustion in air and *in situ* at 600 ºC; time, 4 h.

637 **Figure 9.** TPR profiles of the fresh and regenerated catalysts.

638

Supplementary information

Figure S1. Evolution with TOS of bio-oil oxygenates conversion and yields of products in the SR of bio-oil with Rh/CeO_2-ZrO_2 catalyst in runs of different duration. Reaction conditions: 700 ºC; S/C, 6; space time, 0.15 $g_{catalyst}/g_{bio\text{-}oil}$ h.

Figure S2. SEM images of the fresh (a) and deactivated catalyst at different TOS: 50 min (b), 100 min (c) and 360 min (d).

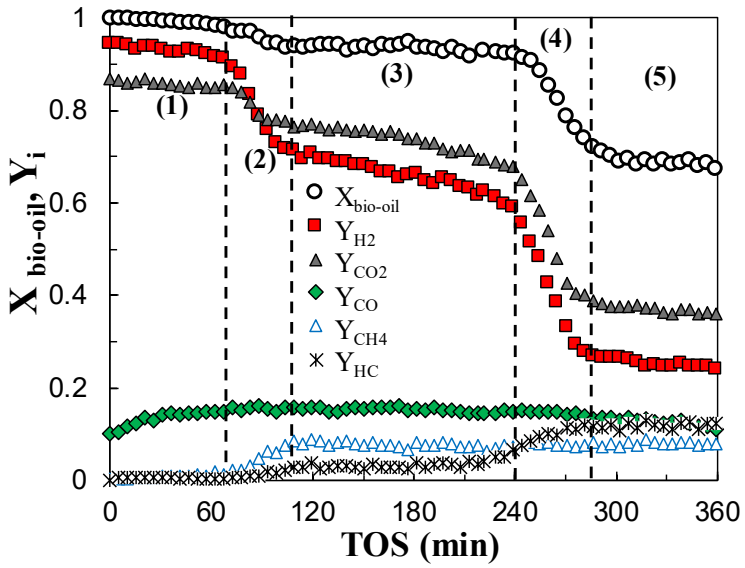
1
0.8
0.6
0.4
0.2
0
0
60
120
180
240
300
360
TOS (min)
X bio-oil, Yi
(1)
(2)
(3)
(4)
(5)
X bio-oil
Y H2
Y CO2
Y CO
Y CH4
Y HC

Figure 1

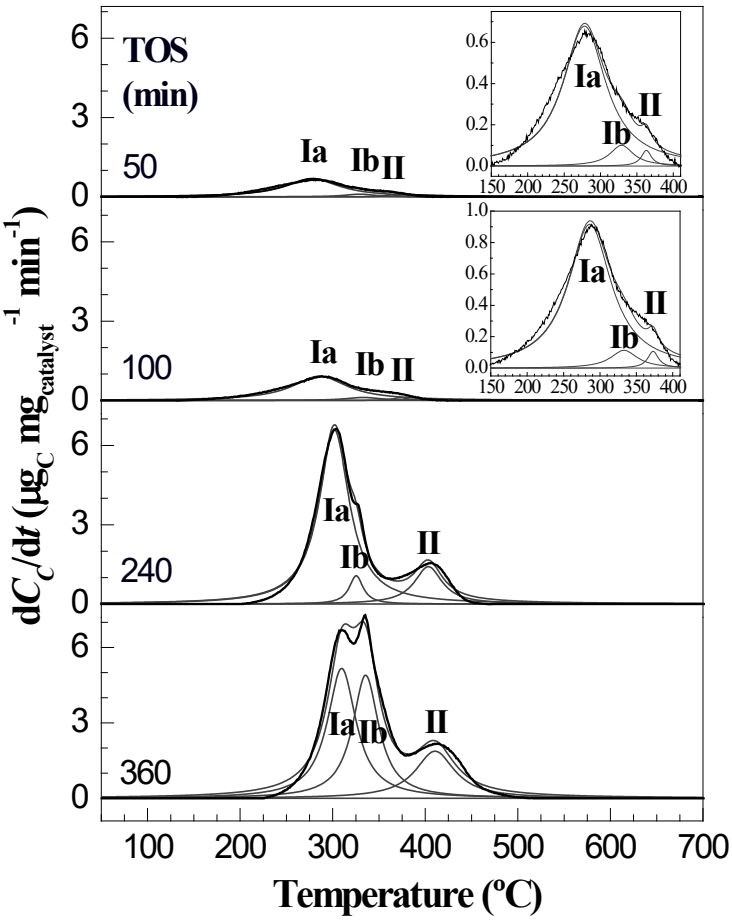
TOS
(min)
50
100
240
360
Ia
Ib
II
dC_C/dt ($\mu g_C\ mg_{catalyst}^{-1}\ min^{-1}$)
Temperature (ºC)

Figure 2

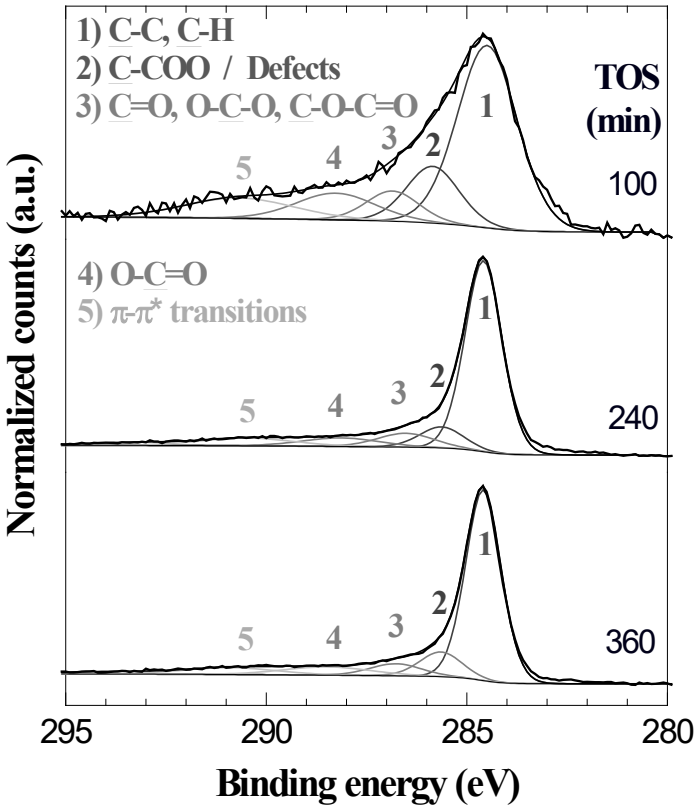
1) C-C, C-H
2) C-COO / Defects
3) C=O, O-C-O, C-O-C=O
4) O-C=O
5) π-π* transitions
TOS (min)
100
240
360
1
2
3
4
5
Normalized counts (a.u.)
295
290
285
280
Binding energy (eV)

Figure 3

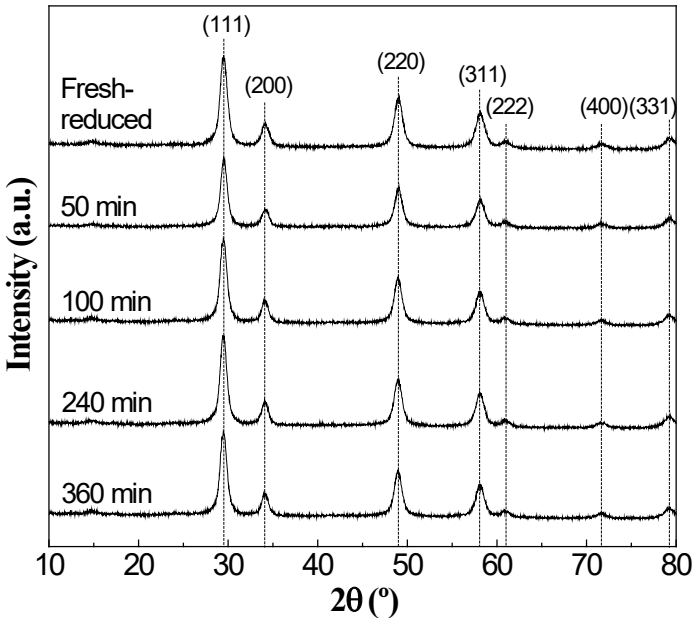
(111)
(200)
(220)
(311)
(222)
(400)
(331)
Fresh-
reduced
50 min
100 min
240 min
360 min
Intensity (a.u.)
10
20
30
40
50
60
70
80
2θ (º)

Figure 4

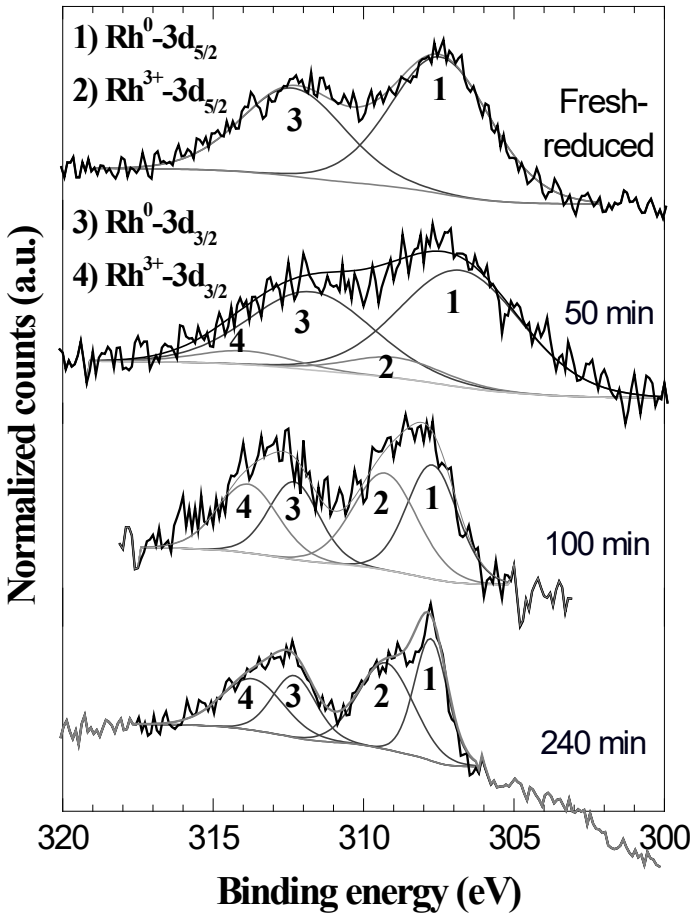
1) Rh0-3d5/2
2) Rh3+-3d5/2
3) Rh0-3d3/2
4) Rh3+-3d3/2
Fresh-reduced
50 min
100 min
240 min
Normalized counts (a.u.)
Binding energy (eV)
320
315
310
305
300

Figure 5

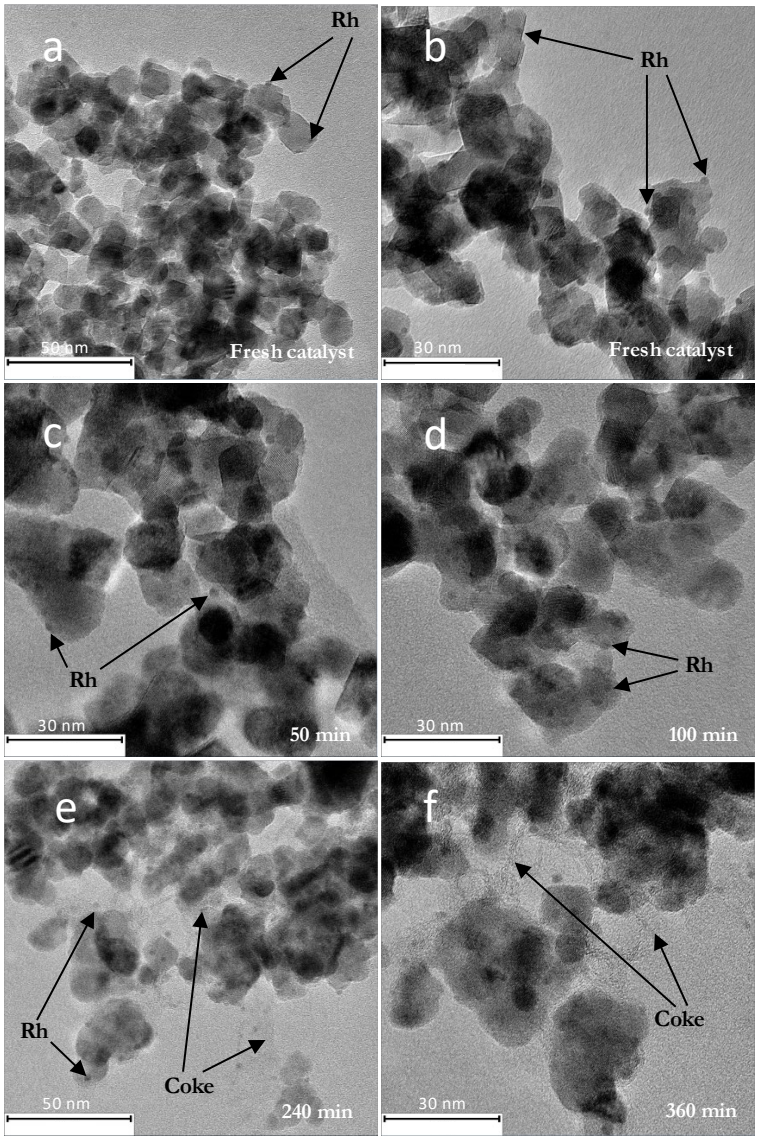
a
Rh
50 nm
Fresh catalyst
b
Rh
30 nm
Fresh catalyst
c
Rh
30 nm
50 min
d
Rh
30 nm
100 min
e
Rh
Coke
50 nm
240 min
f
Coke
30 nm
360 min

Figure 6

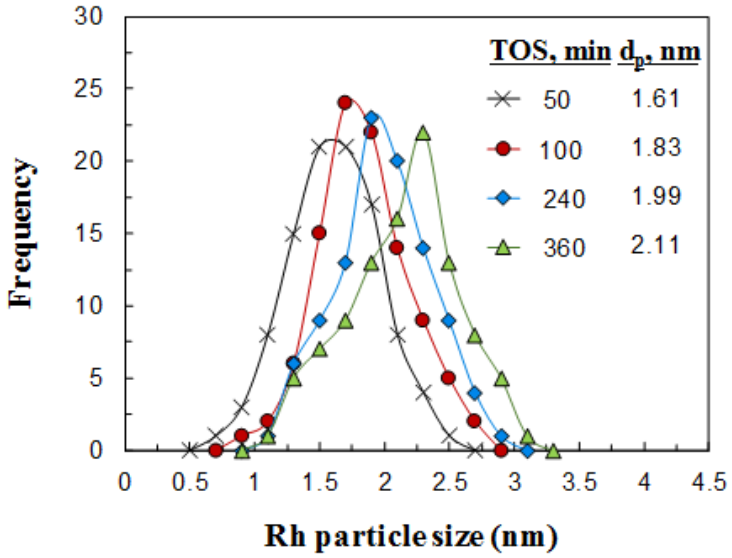
TOS, min
d_p, nm
50 1.61
100 1.83
240 1.99
360 2.11
Frequency
Rh particle size (nm)
0
5
10
15
20
25
30
0 0.5 1 1.5 2 2.5 3 3.5 4 4.5

Figure 7

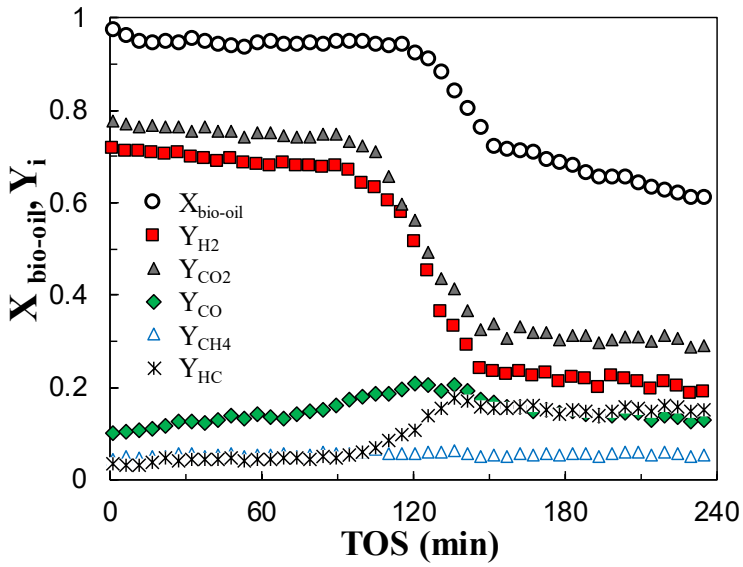
1
0.8
0.6
0.4
0.2
0
0
60
120
180
240
TOS (min)
X bio-oil, Y i
X bio-oil
Y H2
Y CO2
Y CO
Y CH4
Y HC

Figure 8

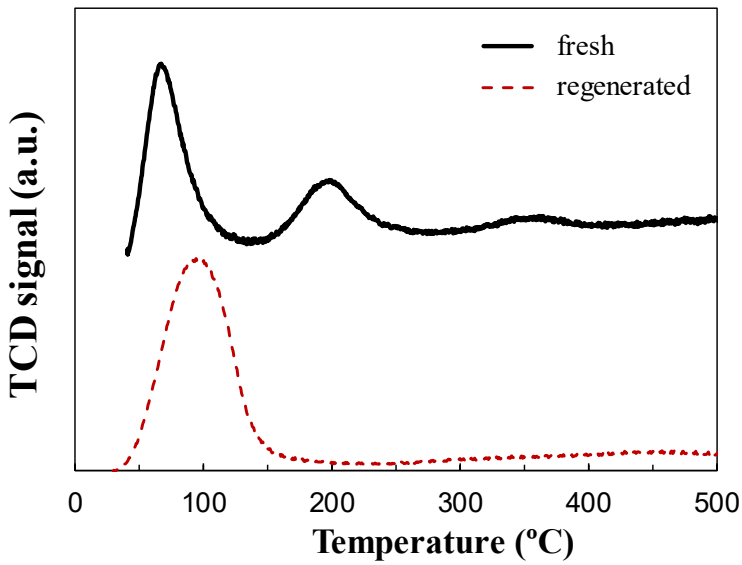
fresh
regenerated
TCD signal (a.u.)
0
100
200
300
400
500
Temperature (ºC)

Figure 9

Table 1. Evolution with TOS of the concentration (in wt %) of oxygenate compounds (water-free basis) in the liquid (analyzed by GC/MS) at the outlet the reforming reactor, under reaction conditions shown in Figure 1.

Compounds	Raw bio-oil	Bio-oil after thermal treatment	50 min	100 min	240 min	360 min
$Y_{oxygenates}$ (%)			1	7	9	30
Ketones	15.55	37.32	58.6	43.05	28.93	23.41
acetone	*1.8*	*10.05*	*58.6*	*43.05*	*8.94*	*7.34*
1-hydroxy-2-propanone	*7.44*	*20.38*	-	-	*14.13*	*12.54*
Acids	35.32	45.96	-	6.28	32.64	36.94
acetic acid	*17.07*	*35.53*	-	*6.28*	*30.92*	*35.23*
Esters	9.41	2.13	-	-	3.22	2.68
Aldehydes	6.24	3.08	-	-	10.03	10.1
Phenols	15.36	6.51	41.4	47.14	17.87	19.34
phenol	*0.31*	*1.77*	*26.5*	*31.26*	*5.23*	*5.57*
2-methylphenol	*0.73*	*1.86*	*11.98*	*10.92*	*4.78*	*5.3*
Ethers	0.48	0.72	-	-	2.09	2.36
Alcohols	2.55	-	-	-	1.6	1.79
Levoglucosan	10.9	2.82	-	2.05	0.97	0.42
Others	4.19	1.46	-	-	-	-
Not identified	-	-	-	1.48	2.65	2.96

Table 2. Deconvolution results of the TPO profiles in Figure 2.

Property	Peak	50 min	100 min	240 min	360 min
T_{max} (ºC)	Ia	278	286	302	310
	Ib	329	333	325	336
	II	363	373	403	411
Coke percentage (wt %, with respect to total coke mass)	Ia	90	90	78	42
	Ib	7	7	6	37
	II	3	3	16	21
Coke content (wt %, with respect to catalyst mass)	Ia	1.44	1.89	6.74	5.42
	Ib	0.12	0.15	0.51	4.70
	II	0.04	0.06	1.34	2.67
	Total	1.6	2.1	8.6	12.8

Table 3. Evolution with TOS of the structural properties and composition (atomic concentrations) of surface coke based on the C 1s region in XPS.

Bond	Position (eV)	Atomic concentration (%)		
		100 min	240 min	360 min
1: C−C, C−H	284.6	21.1	54.9	62.9
2: C−COO and/or defects	285.7	5.8	7.2	9.7
3: C=O, O−C−O, C−O−C=O	286.7	3.1	6.1	5.8
4: O−C=O	288.3	4.1	5.1	6.7
5: ð→ð*	290.7	4.3	5.6	5.9
C 1s		38.4	78.9	91.0
(*1+2*)/C 1s		70.1	78.8	79.7
(*3+4*)/C 1s		18.7	14.2	13.8

Table 4. BET surface area, pore volume and mean pore diameter of the Rh/CeO_2-ZrO_2 catalyst fresh, fresh-reduced, deactivated at different TOS and regenerated.

TOS, min	S_{BET}, m^2g^{-1}	V_{pore}, cm^3g^{-1}	d_{pore}, nm
0 (fresh)	85.7	0.315	17.7
0* (fresh-reduced)	76	0.261	19.2
50	45	0.223	20.0
100	44.5	0.218	19.3
240	37.8	0.166	18.2
360	36.5	0.135	14.1
Regenerated**	40.5	0.212	20.9

*Reduced (700 ºC, 2 h)
**Regenerated (600 ºC, with air)

Table 5. Evolution with TOS of the relative intensities of the Rh bands on the Rh 3d region in XPS, and of the oxidations level of Rh ('Rh^{3+}/Rh^{0}').

Bond	Position (eV)	Fresh-reduced	50 min	100 min	240 min	Regenerated-reduced
Rh^{0}-$3d_{5/2}$	307.4	0.81	0.71	0.23	0.11	0.66
Rh^{3+}-$3d_{5/2}$	309.2	0	0.10	0.25	0.13	0
Rh^{0}-$3d_{3/2}$	312.2	0.54	0.47	0.16	0.08	0.44
Rh^{3+}-$3d_{3/2}$	313.8	0	0.06	0.17	0.09	0
('Rh^{3+}/Rh^{0}')		0	0.14	1.08	1.16	0